

Parameterized quantum comb and simpler circuits for reversing unknown qubit-unitary operations

Yin Mo^{*1}, Lei Zhang^{*1}, Yu-Ao Chen^{*1}, Yingjian Liu¹, Tengxiang Lin¹, and Xin Wang^{†1}

¹Thrust of Artificial Intelligence, Information Hub,
The Hong Kong University of Science and Technology (Guangzhou), Guangdong 511453, China

March 7, 2024

Abstract

Quantum comb is an essential tool for characterizing complex quantum protocols in quantum information processing. In this work, we introduce PQComb, a framework leveraging parameterized quantum circuits to explore the capabilities of quantum combs for general quantum process transformation tasks and beyond. By optimizing PQComb for time-reversal simulations of unknown unitary evolutions, we develop a simpler protocol for unknown qubit unitary inversion that reduces the ancilla qubit overhead from 6 to 3 compared to the existing method in [Yoshida, Soeda, Mura, PRL 131, 120602, 2023]. This demonstrates the utility of quantum comb structures and showcases PQComb's potential for solving complex quantum tasks. Our results pave the way for broader PQComb applications in quantum computing and quantum information, emphasizing its versatility for tackling diverse problems in quantum machine learning.

1 Introduction

In quantum computing, we are capable not only of transforming states but also of transforming processes. Designing quantum circuits to transform input operations has a wide range of applications in quantum computing, quantum information processing, and quantum machine learning. The networks that perform such transformations are known as super-channels [1, 2], which take processes as inputs and output the corresponding transformed process.

In general, all these super-channels can be realized with the quantum comb architecture [1, 2]. Figure 1 illustrates an example where a quantum comb takes m quantum operations as input and outputs a target new operation. Quantum comb is widely applied in solving process transformation problems and optimizing the ultimate achievable performance, including transformations of unitary operations such as inversion [3, 4], complex conjugation, control- U analysis [5], as well as learning tasks [6, 7]. It can also be used for analyzing more general processes [8] and has also inspired structures like the indefinite causal network [9, 10].

However, obtaining the explicit quantum circuit required for the desired transformation is a challenging problem. A major problem of the semidefinite programming (SDP) approach based on the Choi-Jamiołkowski isomorphism is that the dimension of the Choi operator of the quantum comb, i.e., the dimension of the variable in such SDP problems, grows exponentially fast with the increase in the number of comb slots. Another issue is that the SDP ultimately returns the Choi operator of the quantum comb; however, finding a physical implementation of this network, such as converting it into a standard circuit model, is not straightforward.

Drawing from the transformative impact of deep learning in areas such as the game of Go [11] and protein folding prediction [12], we seek to leverage machine learning paradigms to enhance the

^{*}Yin Mo, Lei Zhang, and Yu-Ao Chen contributed equally to this work.

[†]felixxinwang@hkust-gz.edu.cn

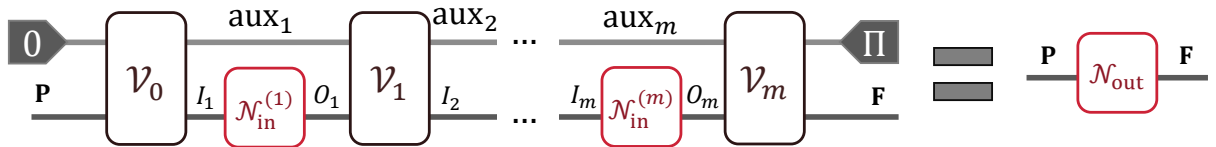


Fig 1: The schematic representation of a sequential quantum comb structure. The notation adopted in this work is presented as follows: \mathbf{P} and \mathbf{F} denote the input and output systems of the main register. I_k and O_k correspond to the input and output systems for the operation in the k -th slot. Additionally, $\mathcal{N}_{\text{in}}^{(k)}$ and \mathcal{N}_{out} denote the k -th input operation and the final output operation highlighted by red boxes, respectively. Each tooth within the comb, corresponding to the k -th position, is characterized by a quantum channel \mathcal{V}_k . aux_k denotes the ancilla system shared by \mathcal{V}_{k-1} and \mathcal{V}_k . At the end of the circuit, the projector Π determines the post-selection of the output auxiliary system. Usually, Π could be selected as the identity matrix, i.e., the output auxiliary system is traced out.

exploration of quantum information technologies. In particular, machine learning has been instrumental in refining quantum processor designs [13, 14, 15, 16] and manipulating quantum entanglement [17, 18]. Also, previous work [19] examined the integration of quantum comb into a quantum auto-encoder within the context of classical cloud computing. In this work, we employ machine learning strategies to tackle the complexities associated with higher-order quantum information transformations. By utilizing Parameterized Quantum Circuits (PQCs), we aim to pioneer new frontiers in the field.

Parameterized quantum circuits, which form a building block of quantum machine learning models, offer a modular approach by decomposing a quantum circuit into an array of single or two-qubit gates, each characterized by tunable parameters [20]. This allows for an iterative optimization process, often employing gradient descent algorithms akin to those found in classical machine learning. This method is more suitable for near-term quantum devices and has been applied in various variational quantum algorithms and quantum machine learning [21, 22, 23]. Due to its structure and its optimization method being similar to classical neural networks, it is also referred to as Quantum Neural Networks.

Based on this idea, we introduce a comprehensive framework named ‘‘PQComb’’, which utilizes PQCs to establish a general quantum comb structure. This framework is applied to the task of transforming quantum processes, where we model the transformation as a quantum comb and employ PQCs to represent the channels of each tooth within the comb. We approach the task as an optimization problem, leveraging classical optimization strategies to optimize the performance of the quantum circuit for the task specified. The optimization is done by adjusting the parameters within this network. Through this framework, we extend PQC into a broader and adaptive quantum neural network with memory to deal with higher-order transformation tasks and, in particular, to develop improved protocols for unitary transformations.

Our methodology is demonstrated to achieve optimal results in the application of reversing unitary operations: specifically, the PQComb can devise a protocol that can perform the unitary inversion by querying four copies of the unitary itself, which has been proven to be the optimal number in terms of usage [4]. Not only does our protocol perform the inversion hardware-efficiently, but it also advances the state of the art by reducing the number of auxiliary qubits required from six [4] to merely three. This application suggests a strong potential for the PQComb to be a useful tool for solving more general tasks.

2 Results

2.1 The PQComb framework

Quantum combs are usually classified as parallel circuits and sequential circuits [2], where the former is a special case of the latter one. Specifically, a sequential quantum comb can be characterized by a sequence of data processing channels $\mathcal{V}_0, \dots, \mathcal{V}_m$ such that \mathcal{V}_j and \mathcal{V}_{j+1} share a memory system. This circuit performs the transformation that takes the input processes $\mathcal{N}_{\text{in}}^{(1)}, \dots, \mathcal{N}_{\text{in}}^{(m)}$ adaptively and output a process \mathcal{N}_{out} as shown in Figure 1. This configuration is particularly noteworthy for its capacity to encapsulate the structure advanced by the quantum signal processing technique [24], an algorithmic

framework that has been instrumental in unifying most well-known quantum algorithms [25]. Furthermore, this architectural paradigm is also applicable to the data re-uploading model in quantum machine learning [26], demonstrating that the Fourier features of a single-qubit quantum unitary can be learned by a data re-uploading QNN model [27].

Despite the integrative potential of quantum combs in quantum computing and quantum machine learning, their applications in algorithm design for specific tasks are impeded by challenges to compile and train. Consider the problem one wants to design a quantum comb to realize the transformation f which outputs a target process with a sequence of input channels, such that

$$f\left(\mathcal{N}_{\text{in}}^{(1)}, \dots, \mathcal{N}_{\text{in}}^{(m)}\right) = \mathcal{N}_{\text{out}}. \quad (1)$$

This problem can be solved by the SDP approach which takes the whole comb's Choi operator $C_{\mathbf{V}}$ as the variable and maximizes its performance function $\text{Tr}[C_{\mathbf{V}}\Omega]$ under comb's constraints, where Ω is the performance operator determined by the given input channels and the target output process [5]. Although the SDP approach allows for the determination of the Choi operator of a feasible quantum comb, the practical compilation of such a comb on actual quantum hardware is hindered by the prohibitive cost associated with non-restricted quantum resources — specifically, the infeasibility of constraining the ranks of channels within the convex optimization framework.

By contrast, in this work, we present the framework of parameterized quantum comb (PQComb) which is a PQC approach that solves the process transformation problem mentioned above. This PQC approach presents a more resource-efficient alternative for quantum computing platforms, owing to the relative ease with which trainable ansatz can be compiled. Specifically, we replace each data processing channel \mathcal{V}_k by PQC, so that the whole comb is now characterized by all adjustable parameters, and the set of which is denoted as θ .

To train the PQComb, different types of loss functions can be chosen based on the problem considered. Once the input channels are fixed, the output process can be obtained by matrix computation directly. Then one choice of the loss function is the dissimilarity between the real output $\widehat{\mathcal{N}}_{\text{out}}(\theta)$ and the target output \mathcal{N}_{out} , denoted as $1 - \mathcal{S}\left(\widehat{\mathcal{N}}_{\text{out}}(\theta), \mathcal{N}_{\text{out}}\right)$ for some computable similarity function \mathcal{S} between processes. We could note that, in contrast to the optimized values in the SDP approach which need to be linear functions, the PQC approach allows us to use more general similarity functions. Optimizing this loss function will provide us with a practical solution to achieve the desired transformation. For the scenario where the input channels are not fixed but sampled from given operation sets, the loss function becomes the average of the dissimilarity, namely the *process-based loss function*

$$\mathcal{L}_p(\theta) = 1 - \frac{1}{N} \sum_{j=1}^N \mathcal{S}\left(\widehat{\mathcal{N}}_{j,\text{out}}(\theta), \mathcal{N}_{j,\text{out}}\right), \quad (2)$$

where $\widehat{\mathcal{N}}_{j,\text{out}}(\theta)$ is the real output process for the j -th input combination sample, and $\mathcal{N}_{j,\text{out}}$ is the expected output for this sample result. As an example, in unitary transformation tasks, the input channel in each slot is usually an unknown unitary gate selected randomly in Haar measure. As shown in Figure 2, computation of \mathcal{L}_p may need to perform sampling and matrix computation to cover all possible selected input channels in each iteration, which encounters diminished training efficacy when the set volume increases.

When the sampling number N is large, and the similarity function can be expressed as a linear equation in terms of the PQComb's Choi operator $C_{\mathbf{V}}(\theta)$ as

$$\mathcal{S}\left(\widehat{\mathcal{N}}_{j,\text{out}}(\theta), \mathcal{N}_{j,\text{out}}\right) = \text{Tr}[C_{\mathbf{V}}(\theta)\Omega_j], \quad (3)$$

where Ω_j is the performance operator determined by $\widehat{\mathcal{N}}_{j,\text{in}}^{(1)}, \dots, \mathcal{N}_{j,\text{in}}^{(m)}$ and $\mathcal{N}_{j,\text{out}}$, we propose an alternative loss function to overcome the sampling problem, namely the *comb-based loss function*.

$$\mathcal{L}_c(\theta) = 1 - \text{Tr}[C_{\mathbf{V}}(\theta)\Omega], \quad (4)$$

where $\Omega = \frac{1}{N} \sum_{j=1}^N \Omega_j$. This loss function incorporates the features of both PQC and quantum comb. As illustrated in Figure 2, the Choi operator $C_{\mathbf{V}}(\theta)$ can be calculated by inserting unnormalized maximally

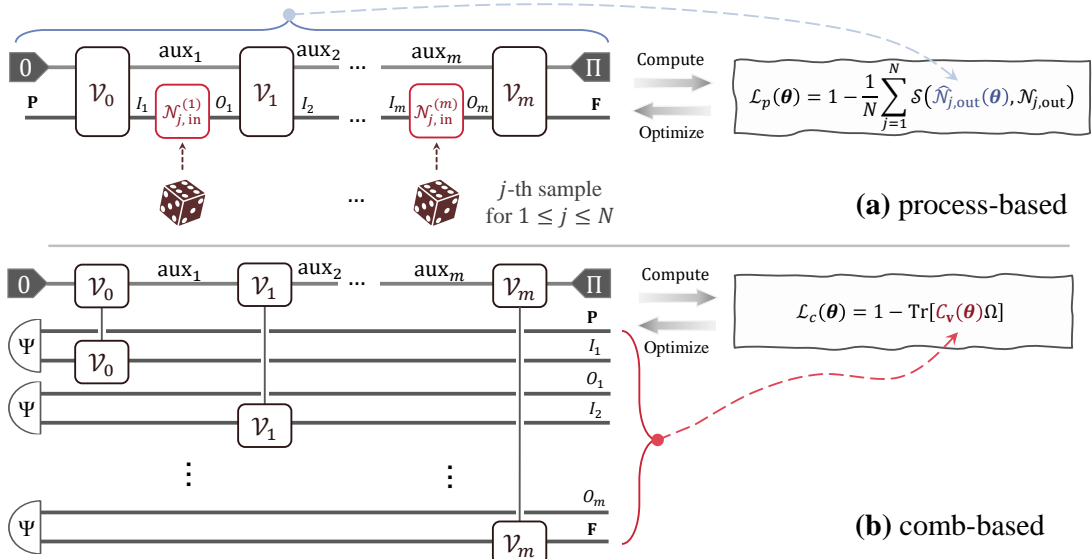


Fig 2: The overview of training formalism for the parameterized quantum comb framework. Within this scheme, \mathcal{V}_k is now parameterized and remains tunable to adjustments during the optimization phase, and θ is denoted as the vector of all parameters in this PQComb. **(a)** describes how the PQComb trains the protocol using the process-based loss function \mathcal{L}_p , which is computed by the average dissimilarity between the sampled output process $\hat{\mathcal{N}}_{j,\text{out}}(\theta)$ and the target process $\mathcal{N}_{j,\text{out}}$. **(b)** describes how the PQComb trains the protocol using the comb-based loss function \mathcal{L}_c , which optimizes the Choi operator of the circuit $C_{\mathbf{V}}(\theta)$ using the performance operator Ω . Here $\Psi = \sum_{i,j} |ii\rangle\langle jj|$ is the unnormalized maximally entangled state.

entangled states to all input systems of the parameterized comb. Since the performance operator Ω is determined by the input channels and the target output, it allows for pre-computation, thus avoiding the need for sampling at every iteration.

In the next section, we show the process of solving specific problems using the PQComb framework by designing a unitary inversion protocol, i.e., $f(U^{(1)}, \dots, U^{(m)}) = U^{-1}$. We will first introduce the task of unitary inversion, followed by detailing the process of obtaining the final solution using the PQComb. Through this case study, we could see the potential of PQComb to yield optimal solutions and assist us in designing better protocols.

2.2 Application to Unitary Inversion

The time evolution of a closed quantum system can be characterized by a unitary operator $U = e^{-iHt}$ with a Hamiltonian H and time t . One can always reverse this transformation via the inverse operation $U^{-1} = e^{iHt}$. The reversible nature of quantum unitary reveals a fundamental distinction between quantum computing and classical computing, which also mirrors the time-reversal symmetry of the underlying quantum mechanics.

The simulation of time-reversed quantum unitary evolution is not only a conceptual cornerstone in the realm of quantum information [28], but it also serves as a key technology for the manipulation of quantum systems. This intricate process is pivotal for measuring out-of-time-order correlators [29, 30, 31], which serve as diagnostics for quantum chaos and entanglement dynamics. Moreover, the ability to reverse an unknown unitary evolution is an important building block for quantum algorithms (e.g., quantum singular value transformation [32]), underscoring its significance in advancing quantum computational capabilities.

Reversing an unknown unitary evolution presents a significant challenge since it typically requires complete knowledge of the system but the information of a physics system in nature is often beyond our grasp. For the implementation of the inverse operation, one must have an exact characterization of the unitary transformation or the underlying Hamiltonian. However, quantum process tomography, the standard technique for such characterization of unitary operation, demands an impractically large

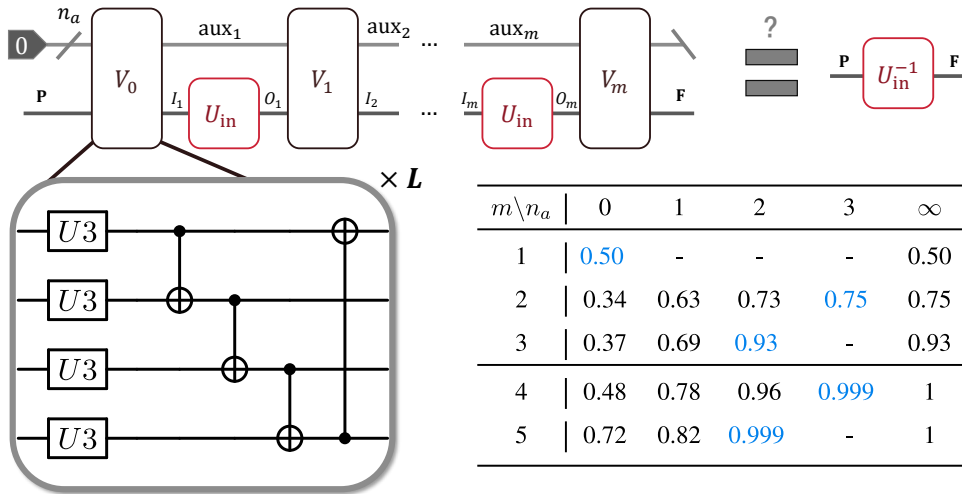


Fig 3: The sequential circuit structure used in PQComb for the single-qubit unitary inversion task. Here m , n_a are the number of slots and ancilla qubits, respectively. The table below the circuit summarizes the maximal average fidelity $\text{Tr}[C_{\mathbf{V}}(\theta)\Omega]$ obtained by the PQComb, for different pairs of (m, n_a) . Here ∞ refers to the case when the number of ancilla is unlimited, where the optimal value is given in [4].

number of measurements to fully describe a quantum process [33, 34, 35, 36]. This requirement renders the exact reversal of a general unknown unitary operation impractical, as the conventional approach of learning and inverting is resource-prohibitive.

While process tomography is challenging, simulating the unitary inverse U^{-1} using the original unitary operation U is still possible. Higher-order transformations of quantum dynamics provide a potentially feasible approach for transforming an unknown unitary to its inverse. In particular, Ref. [37] introduces a probabilistic universal quantum algorithm that executes the exact inversion of an unknown unitary operation. Furthermore, Ref. [4] uses 6 ancilla qubits to establish the first deterministic and exact protocol for reversing any unknown qubit-unitary operations. However, it still remains an open question on whether the number of ancilla qubits can be further reduced.

In this section, we answer this question by applying PQComb to the unitary inversion task. We first optimize with the ansatz shown in Figure 3, obtaining a circuit close to perfect. This ansatz is commonly used in VQA, where the channel in each tooth is formed by repeatedly applying complex entangled layers [38]. The projectors for the output auxiliary systems are specified as $\Pi = I^{\otimes n_a}$, where n_a is the number of ancilla qubits. After achieving a solution close to perfect, we further refine our optimization based on the current circuit, resulting in a deterministic and exact protocol, as illustrated in Figure 4.

In this task, we choose \mathcal{L}_c in Eq. (4) as our loss function where the performance operator Ω is given as by [39]:

$$\Omega = \int_{\text{Haar}} dU |U^{-1}\rangle\rangle\langle\langle U^{-1}|_{\mathbf{P},\mathbf{F}} \otimes |\bar{U}\rangle\rangle\langle\langle \bar{U}|_{I_1,O_1} \otimes \dots \otimes |\bar{U}\rangle\rangle\langle\langle \bar{U}|_{I_m,O_m} \quad (5)$$

$$\approx \frac{1}{N} \sum_{k=1}^N |U_k^{-1}\rangle\rangle\langle\langle U_k^{-1}|_{\mathbf{P},\mathbf{F}} \otimes |\bar{U}_k\rangle\rangle\langle\langle \bar{U}_k|_{I,O}. \quad (6)$$

Here $|U\rangle\rangle = \sum_j (U \otimes I)|j\rangle|j\rangle$ corresponds to the Choi operator of unitary gate U , and the set $\{U_k\}_{k=1}^N$ is randomly sampled from the special unitary group $\mathfrak{su}(2)$ with $N = 10^3$. One can then follow the optimization procedure in Figure 2 to experimentally find the protocol with the optimal loss function for each setting (m, n_a) , as summarized in Figure 3. Notably, the average fidelity obtained by the PQComb matches the optimal value for $1 \leq m \leq 5$ within a tolerance of $1 \cdot 10^{-3}$ [4].

The data presented in Figure 3 indicates that by utilizing three ancilla qubits and four applications of the unitary operator U_{in} , PQComb is capable of providing a deterministic and nearly exact protocol to approximate U_{in}^{-1} . Upon a thorough analysis of the protocol, we postulate that for each input U_{in} , the surrounded four-qubit unitaries V_{j-1} and V_j potentially include encoding and decoding operations

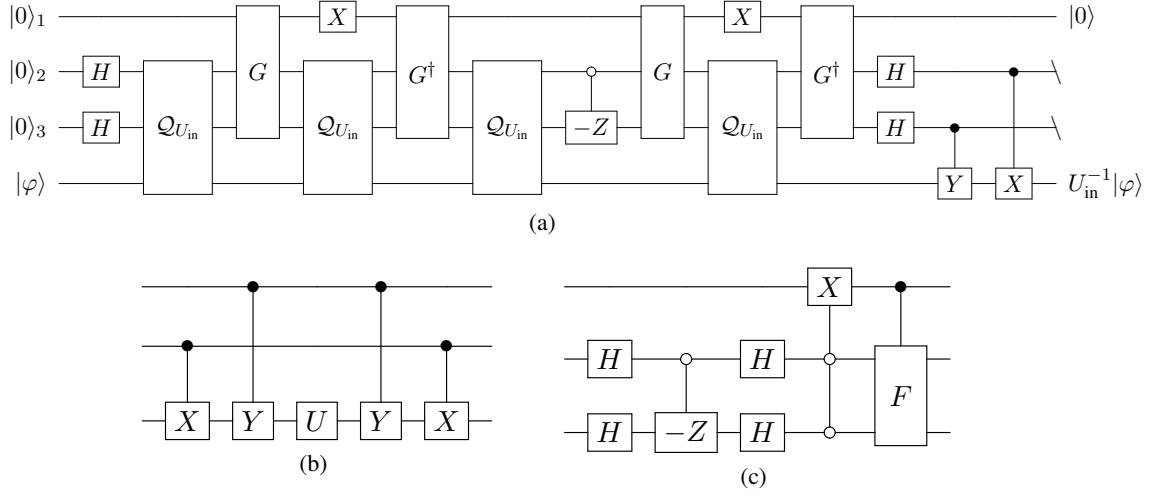


Fig 4: The proposed unitary inversion protocol for arbitrary single-qubit unitary U_{in} . **(a)** One can use 3 ancilla qubits and 4 queries of U_{in} to realize U_{in}^{-1} . **(b)** Circuit implementation of $Q_{U_{in}}$. **(c)** Circuit implementation of G , where F is a two-qubit unitary such that $F|00\rangle = (|01\rangle + |10\rangle + |11\rangle)/\sqrt{3}$.

facilitated by control Pauli gates, enabling the ancilla qubits to produce a specific linear combination of U acting on the target qubit, which ultimately transforms into the action of U_{in}^{-1} . This conjecture leads to a more streamlined training ansatz, which in turn suppresses the loss function to 10^{-6} . The ansatz employed by PQComb is illustrated by Figure S1a in the Appendix A, giving our principal theoretical contribution:

Theorem 1 *There exists a quantum circuit C_{IV} implementing U^{-1} by 3 ancilla qubits and 4 calls of a single-qubit unitary U , such that*

$$\text{Tr}_{23} [C_{IV}(U)|000\rangle_{123}|\psi\rangle] = |0\rangle_1 \otimes U^{-1}|\psi\rangle. \quad (7)$$

Sketch of Proof. The existence of C_{IV} is evidenced by the circuit in Figure 4. In particular, for $U_{in} \in \mathfrak{su}(2)$, a decomposition on Pauli basis is $U_{in} = \cos \frac{\theta}{2} I - i \sin \frac{\theta}{2} \vec{n} \cdot \vec{\sigma}$, with $\vec{n} = (n_x, n_y, n_z)$ respective to the coefficients of Pauli operators. The output state of this circuit satisfies

$$|\Psi_{OUT}\rangle = \frac{1}{2}|0\rangle \otimes \left(\cos \frac{\theta}{2} |00\rangle - i \sin \frac{\theta}{2} n_y |01\rangle - i \sin \frac{\theta}{2} n_x |10\rangle - i \sin \frac{\theta}{2} n_z |11\rangle \right) \otimes U^{-1}|\varphi\rangle \quad (8)$$

and hence, the statement follows. More details are deferred to Appendix B.

An alternative training result of the PQComb also indicates that all ancilla qubits can be reset rather than traced out, by using one more slot, as shown in Figure S1b. This is summarized in the following corollary.

Corollary 2 *There exists a quantum circuit C_V implementing U^{-1} by 3 ancilla qubits and 5 calls of a single-qubit unitary U , such that*

$$C_V(U)|000, \psi\rangle = |000\rangle \otimes U^{-1}|\psi\rangle. \quad (9)$$

3 Concluding remarks

We developed PQComb for exploring the capabilities of quantum combs in transforming quantum processes. Compared to the traditional SDP method, this approach has the advantages in providing more flexible loss functions tailored to different tasks and resources, designing practical circuits for actual implementation, and customizing the search space by appropriate parameterization.

One significant contribution from our work is the creation of a more straightforward approach to reverse unknown qubit-unitary operations, derived from the PQComb’s optimization for this specific task. This new protocol simplifies the circuit complexity and enhances the efficiency of qubit-unitary inversion by halving the circuit width. Such a reduction not only highlights the practical value of quantum comb structures but also illustrates PQComb’s capacity for generating cutting-edge quantum protocols and algorithms.

Future research directions include exploring ansatzes for quantum combs with different structures to solve various types of problems and developing novel quantum algorithms with the aid of PQComb. Here, we also want to note that the task of reversing dimension-2 unitary operations discussed in this work is subsequently extended to arbitrary dimensions in [40]. We believe the results in this paper could pave the way for the application of the parametrized quantum combs across quantum computing and machine learning domains, opening up new possibilities for future research and development in these fields.

Acknowledgement

Y. M., L. Z., and Y.-A. Chen contributed equally to this work. We would like to thank Xuanqiang Zhao and Yu Gan for their helpful comments. This work was supported by the Start-up Fund (No. G0101000151) from The Hong Kong University of Science and Technology (Guangzhou), the Guangdong Provincial Quantum Science Strategic Initiative (No. GDZX2303007), and the Education Bureau of Guangzhou Municipality.

References

- [1] G. Chiribella, G. M. D’Ariano, and P. Perinotti. Transforming quantum operations: Quantum supermaps. *Europhysics Letters*, 83(3):30004, July 2008.
- [2] Giulio Chiribella, Giacomo Mauro D’Ariano, and Paolo Perinotti. Quantum circuits architecture. *Physical Review Letters*, 101(6):060401, August 2008.
- [3] Marco Túlio Quintino, Qingxiuxiong Dong, Atsushi Shimbo, Akihito Soeda, and Mio Murao. Reversing unknown quantum transformations: Universal quantum circuit for inverting general unitary operations. *Physical Review Letters*, 123(21):210502, November 2019.
- [4] Satoshi Yoshida, Akihito Soeda, and Mio Murao. Reversing Unknown Qubit-Unitary Operation, Deterministically and Exactly. *Physical Review Letters*, 131(12), 2023.
- [5] Giulio Chiribella and Daniel Ebler. Optimal quantum networks and one-shot entropies. *New Journal of Physics*, 18(9):093053, September 2016.
- [6] Alessandro Bisio, Giulio Chiribella, Giacomo Mauro D’Ariano, Stefano Facchini, and Paolo Perinotti. Optimal quantum learning of a unitary transformation. *Physical Review A*, 81(3):032324, March 2010.
- [7] Michal Sedlák, Alessandro Bisio, and Mário Ziman. Optimal probabilistic storage and retrieval of unitary channels. *Physical Review Letters*, 122(17):170502, May 2019.
- [8] Chengkai Zhu, Yin Mo, Yu-Ao Chen, and Xin Wang. Reversing Unknown Quantum Processes via Virtual Combs: for Channels with Limited Information. *arXiv preprint arXiv:2401.04672*, 2024.
- [9] Giulio Chiribella, Giacomo Mauro D’Ariano, Paolo Perinotti, and Benoit Valiron. Quantum computations without definite causal structure. *Physical Review A*, 88(2):022318, August 2013.
- [10] Ognjan Oreshkov, Fabio Costa, and Časlav Brukner. Quantum correlations with no causal order. *Nature Communications*, 3(1):1092, October 2012.

- [11] David Silver, Aja Huang, Chris J Maddison, Arthur Guez, Laurent Sifre, George Van Den Driessche, Julian Schrittwieser, Ioannis Antonoglou, Veda Panneershelvam, and Marc Lanctot. Mastering the game of Go with deep neural networks and tree search. *Nature*, 529(7587):484–489, 2016.
- [12] John Jumper, R Evans, A Pritzel, T Green, M Figurnov, K Tunyasuvunakool, O Ronneberger, R Bates, A Zidek, and A Bridgland. High accuracy protein structure prediction using deep learning. *Fourteenth Critical Assessment of Techniques for Protein Structure Prediction (Abstract Book)*, 22:24, 2020.
- [13] Sandeep Mavadia, Virginia Frey, Jarrah Sastrawan, Stephen Dona, and Michael J Biercuk. Prediction and real-time compensation of qubit decoherence via machine learning. *Nature Communications*, 8(1):14106, apr 2017.
- [14] Kwok Ho Wan, Oscar Dahlsten, Hlér Kristjánsson, Robert Gardner, and M. S. Kim. Quantum generalisation of feedforward neural networks. *npj Quantum Information*, 3(1):36, dec 2017.
- [15] Dawei Lu, Keren Li, Jun Li, Hemant Katiyar, Annie Jihyun Park, Guanru Feng, Tao Xin, Hang Li, Guilu Long, and Aharon Brodutch. Enhancing quantum control by bootstrapping a quantum processor of 12 qubits. *npj Quantum Information*, 3(1):1–7, 2017.
- [16] Murphy Yuezhen Niu, Sergio Boixo, Vadim N. Smelyanskiy, and Hartmut Neven. Universal quantum control through deep reinforcement learning. *npj Quantum Information*, 5(1):33, dec 2019.
- [17] Julius Wallnöfer, Alexey A. Melnikov, Wolfgang Dür, and Hans J. Briegel. Machine Learning for Long-Distance Quantum Communication. *PRX Quantum*, 1(1):010301, sep 2020.
- [18] Xuanqiang Zhao, Benchi Zhao, Zihe Wang, Zhixin Song, and Xin Wang. Practical distributed quantum information processing with loccnet. *npj Quantum Information*, 7(1):159, November 2021.
- [19] Yan Zhu, Ge Bai, Yuexuan Wang, Tongyang Li, and Giulio Chiribella. Quantum autoencoders for communication-efficient cloud computing. *Quantum Machine Intelligence*, 5(2):27, December 2023.
- [20] Marcello Benedetti, Erika Lloyd, Stefan Sack, and Mattia Fiorentini. Parameterized quantum circuits as machine learning models. *Quantum Science and Technology*, 4(4):043001, nov 2019.
- [21] Alberto Peruzzo, Jarrod McClean, Peter Shadbolt, Man-Hong Yung, Xiao-Qi Zhou, Peter J Love, Alán Aspuru-Guzik, and Jeremy L O’Brien. A variational eigenvalue solver on a photonic quantum processor. *Nature Communications*, 5:4213, 2014.
- [22] Jarrod R McClean, Jonathan Romero, Ryan Babbush, and Alán Aspuru-Guzik. The theory of variational hybrid quantum-classical algorithms. *New Journal of Physics*, 18(2):023023, 2016.
- [23] M. Cerezo, Andrew Arrasmith, Ryan Babbush, Simon C. Benjamin, Suguru Endo, Keisuke Fujii, Jarrod R. McClean, Kosuke Mitarai, Xiao Yuan, Lukasz Cincio, and Patrick J. Coles. Variational quantum algorithms. *Nature Reviews Physics*, 3(9):625–644, August 2021.
- [24] Guang Hao Low, Theodore J. Yoder, and Isaac L. Chuang. The methodology of resonant equiangular composite quantum gates. *Physical Review X*, 6(4):041067, December 2016.
- [25] John M. Martyn, Zane M. Rossi, Andrew K. Tan, and Isaac L. Chuang. A grand unification of quantum algorithms. *PRX Quantum*, 2(4):040203, December 2021.
- [26] Adrián Pérez-Salinas, Alba Cervera-Lierta, Elies Gil-Fuster, and José I. Latorre. Data re-uploading for a universal quantum classifier. *Quantum*, 4:226, February 2020.
- [27] Zhan Yu, Hongshun Yao, Mujin Li, and Xin Wang. Power and limitations of single-qubit native quantum neural networks. In *36th Conference on Neural Information Processing Systems (NeurIPS 2022)*, 2022.

- [28] Yakir Aharonov, Jeeva Anandan, Sandu Popescu, and Lev Vaidman. Superpositions of time evolutions of a quantum system and a quantum time-translation machine. *Physical Review Letters*, 64(25):2965, 1990.
- [29] Juan Maldacena, Stephen H Shenker, and Douglas Stanford. A bound on chaos. *Journal of High Energy Physics*, 2016(8):1–17, 2016.
- [30] Jun Li, Ruihua Fan, Hengyan Wang, Bingtian Ye, Bei Zeng, Hui Zhai, Xinhua Peng, and Jiangfeng Du. Measuring out-of-time-order correlators on a nuclear magnetic resonance quantum simulator. *Physical Review X*, 7(3):31011, 2017.
- [31] Martin Gärttner, Justin G Bohnet, Arghavan Safavi-Naini, Michael L Wall, John J Bollinger, and Ana Maria Rey. Measuring out-of-time-order correlations and multiple quantum spectra in a trapped-ion quantum magnet. *Nature Physics*, 13(8):781–786, 2017.
- [32] András Gilyén, Yuan Su, Guang Hao Low, and Nathan Wiebe. Quantum singular value transformation and beyond: Exponential improvements for quantum matrix arithmetics. In *Proceedings of the 51st Annual ACM SIGACT Symposium on Theory of Computing*, pages 193–204, Phoenix AZ USA, June 2019. ACM.
- [33] Charles H Baldwin, Amir Kalev, and Ivan H Deutsch. Quantum process tomography of unitary and near-unitary maps. *Physical Review A*, 90(1):12110, jul 2014.
- [34] Gus Gutoski and Nathaniel Johnston. Process tomography for unitary quantum channels. *Journal of Mathematical Physics*, 55(3):32201, 2014.
- [35] M Mohseni, A T Rezakhani, and D A Lidar. Quantum-process tomography: Resource analysis of different strategies. *Physical Review A*, 77(3):032322, mar 2008.
- [36] Jeongwan Haah, Robin Kothari, Ryan O’Donnell, and Ewin Tang. Query-optimal estimation of unitary channels in diamond distance. In *2023 IEEE 64th Annual Symposium on Foundations of Computer Science (FOCS)*, pages 363–390. IEEE, 2023.
- [37] Marco Túlio Quintino, Qingxiuxiong Dong, Atsushi Shimbo, Akihito Soeda, and Mio Muraō. Probabilistic exact universal quantum circuits for transforming unitary operations. *Physical Review A*, 100(6):062339, dec 2019.
- [38] Paddle Quantum, 2020.
- [39] Marco Túlio Quintino and Daniel Ebler. Deterministic transformations between unitary operations: Exponential advantage with adaptive quantum circuits and the power of indefinite causality. *Quantum*, 6:679, March 2022.
- [40] Yu-Ao Chen, Yin Mo, Yingjian Liu, Lei Zhang, and Xin Wang. Quantum advantage in reversing unknown unitary evolutions, 2024. to be appeared on arXiv.

Supplementary Material

A Training Ansatz in Unitary Inversion Task

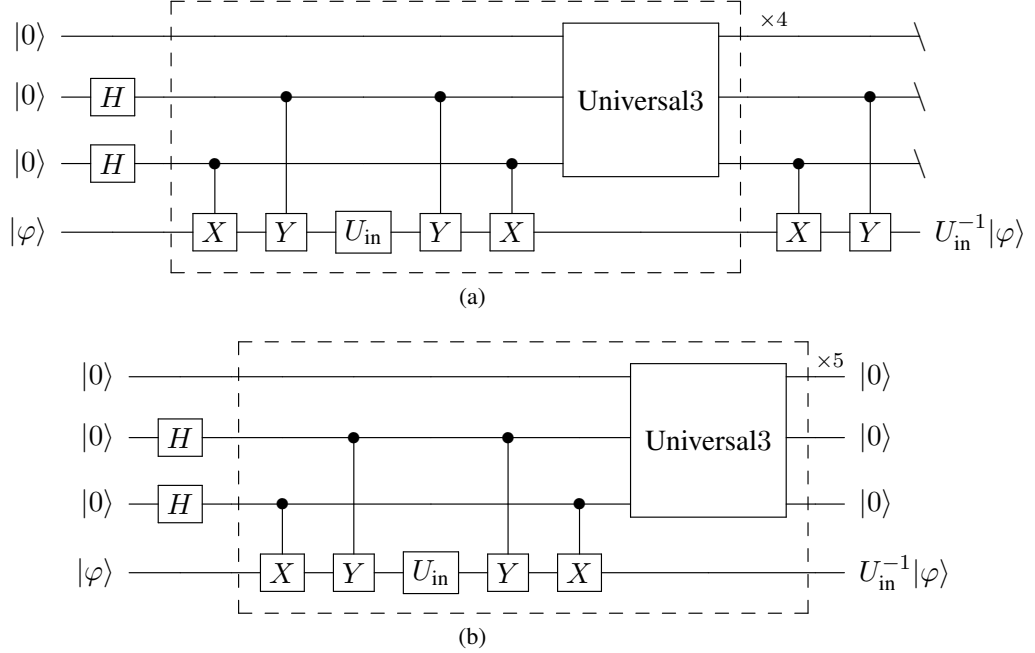


Fig S1: Two trainable ansatzes in PQComb that reduce to Figure S2a and Figure S2b.

B Proof of Theorem 1 and Corollary 2

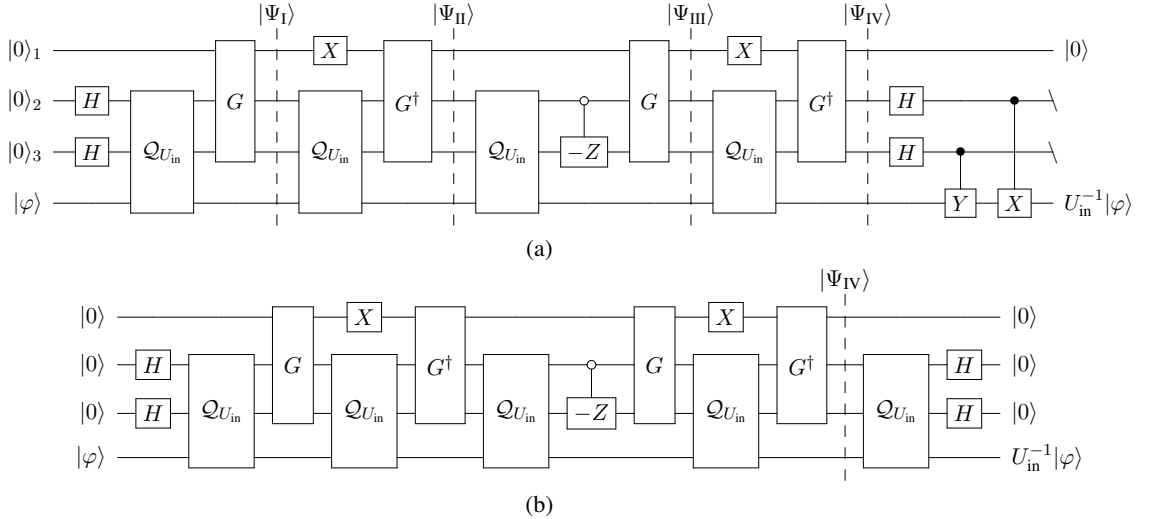


Fig S2: (a) An example of implementing C_{IV} in Theorem 1. (b) An example of implementing C_V in Corollary 2.

Theorem 1 C_{IV} in Figure S2a satisfies

$$\text{Tr}_{23} [C_{IV}(U)|000\rangle_{123}|\psi\rangle] = |0\rangle_1 \otimes U^{-1}|\psi\rangle. \quad (S1)$$

Proof Without loss of generality, suppose the determinant of U is 1 i.e., $U \in \mathfrak{su}(2)$. Without Notice that there is a linear relation between qubit unitary $U \in \mathfrak{su}(2)$ and its inversion

$$2U^{-1} = XUX + YUY + ZUZ - U. \quad (S2)$$

In the rest of proof, we analyze the states at four stages in Fig. S2a.

The circuit is initialized with the input state $|\Psi_{\text{in}}\rangle$, during the first step

$$|\Psi_{\text{in}}\rangle \xrightarrow{H} |0\rangle \otimes |+\rangle \otimes |+\rangle \otimes |\varphi\rangle, \quad (\text{S3})$$

$$\xrightarrow{\mathcal{Q}_{U_{\text{in}}}} \frac{1}{2} |0\rangle \otimes (|00\rangle \otimes U|\varphi\rangle + |01\rangle \otimes XU^{\dagger}X|\varphi\rangle + |10\rangle \otimes YUY|\varphi\rangle + |11\rangle \otimes ZUZ|\varphi\rangle), \quad (\text{S4})$$

$$\xrightarrow{O} \frac{1}{2} |0\rangle \otimes (|00\rangle \otimes U^{-1}|\varphi\rangle + |01\rangle \otimes XU^{-1}X|\varphi\rangle + |10\rangle \otimes YU^{-1}Y|\varphi\rangle + |11\rangle \otimes ZU^{-1}Z|\varphi\rangle). \quad (\text{S5})$$

We make the following notation to make the deduction smoother:

$$|0^{\perp}\rangle = \frac{(|01\rangle + |10\rangle + |11\rangle)}{\sqrt{3}} \quad (\text{S6})$$

$$O = H^{\otimes 2} (-|0\rangle\langle 0| \otimes Z + |1\rangle\langle 1| \otimes I) \quad (\text{S7})$$

Applying the rest part of the defined block G in Fig. 4a(d) gives

$$|\Psi_{\text{I}}\rangle = \frac{1}{2} |1\rangle \otimes |0^{\perp}\rangle \otimes U^{-1}|\varphi\rangle + \frac{1}{2} |0\rangle \otimes (|01\rangle \otimes XU^{-1}X|\varphi\rangle + \quad (\text{S8})$$

$$|10\rangle \otimes YU^{-1}Y|\varphi\rangle + \quad (\text{S9})$$

$$|11\rangle \otimes ZU^{-1}Z|\varphi\rangle), \quad (\text{S10})$$

$$\xrightarrow{X} \frac{1}{2} |0\rangle \otimes |0^{\perp}\rangle \otimes U^{-1}|\varphi\rangle + \frac{1}{2} |1\rangle \otimes (|01\rangle \otimes XU^{-1}X|\varphi\rangle + \quad (\text{S11})$$

$$|10\rangle \otimes YU^{-1}Y|\varphi\rangle + \quad (\text{S12})$$

$$|11\rangle \otimes ZU^{-1}Z|\varphi\rangle), \quad (\text{S13})$$

$$\xrightarrow{\mathcal{Q}_{U_{\text{in}}}} \frac{-\sqrt{3}}{2} |1\rangle \otimes |0^{\perp}\rangle \otimes |\varphi\rangle - \frac{1}{2\sqrt{3}} |0\rangle \otimes (|01\rangle \otimes XU^{\dagger}XU^{-1}|\varphi\rangle + \quad (\text{S14})$$

$$|10\rangle \otimes YUYU^{-1}|\varphi\rangle + \quad (\text{S15})$$

$$|11\rangle \otimes ZUZU^{-1}|\varphi\rangle). \quad (\text{S16})$$

Applying G^{\dagger} , it turns to

$$|\Psi_{\text{II}}\rangle = \frac{1}{2\sqrt{3}} |0\rangle \otimes [|00\rangle \otimes (U^{-1} - U) + \quad (\text{S17})$$

$$|01\rangle \otimes (U + XU^{-1}X) + \quad (\text{S18})$$

$$|10\rangle \otimes (U + YU^{-1}Y) + \quad (\text{S19})$$

$$|11\rangle \otimes (U + ZU^{-1}Z)]U^{-1}|\varphi\rangle. \quad (\text{S20})$$

Notice that $\sigma_i U \sigma_i (U + \sigma_i U^{-1} \sigma_i) U^{-1} = U^{-1} + \sigma_i U \sigma_i$, then

$$\mathcal{Q}_{U_{\text{in}}} |\Psi_{\text{II}}\rangle = \frac{1}{2\sqrt{3}} |0\rangle \otimes [|00\rangle \otimes (U^{-1} - U) + \quad (\text{S21})$$

$$|01\rangle \otimes (U^{-1} + XU^{\dagger}X) + \quad (\text{S22})$$

$$|10\rangle \otimes (U^{-1} + YUY) + \quad (\text{S23})$$

$$|11\rangle \otimes (U^{-1} + ZUZ)]|\varphi\rangle, \quad (\text{S24})$$

$$\xrightarrow{c(-Z)} \frac{1}{2\sqrt{3}} |0\rangle \otimes [|00\rangle \otimes (U - U^{-1}) + \quad (\text{S25})$$

$$|01\rangle \otimes (U^{-1} + XU^{\dagger}X) + \quad (\text{S26})$$

$$|10\rangle \otimes (U^{-1} + YUY) + \quad (\text{S27})$$

$$|11\rangle \otimes (U^{-1} + ZUZ)]|\varphi\rangle, \quad (\text{S28})$$

$$\xrightarrow{O} \frac{-1}{2\sqrt{3}} |0\rangle \otimes [|00\rangle \otimes (3U^{-1}) + \quad (\text{S29})$$

$$|01\rangle \otimes (XU^{-1}X) + \quad (\text{S30})$$

$$|10\rangle \otimes (YU^{-1}Y) + \quad (\text{S31})$$

$$|11\rangle \otimes (ZU^{-1}Z)]|\varphi\rangle. \quad (\text{S32})$$

$$(\text{S33})$$

Applying the rest of second G gives

$$|\Psi_{\text{III}}\rangle = \frac{-\sqrt{3}}{2}|0\rangle \otimes |0^\perp\rangle \otimes U^{-1}|\varphi\rangle - \frac{1}{2\sqrt{3}}|1\rangle \otimes (|01\rangle \otimes XU^{-1}X|\varphi\rangle + \quad (S34)$$

$$|10\rangle \otimes YU^{-1}Y|\varphi\rangle + \quad (S35)$$

$$|11\rangle \otimes ZU^{-1}Z|\varphi\rangle), \quad (S36)$$

$$\xrightarrow{X} \frac{-\sqrt{3}}{2}|1\rangle \otimes |0^\perp\rangle \otimes U^{-1}|\varphi\rangle - \frac{1}{2\sqrt{3}}|0\rangle \otimes (|01\rangle \otimes XU^{-1}X|\varphi\rangle + \quad (S37)$$

$$|10\rangle \otimes YU^{-1}Y|\varphi\rangle + \quad (S38)$$

$$|11\rangle \otimes ZU^{-1}Z|\varphi\rangle), \quad (S39)$$

$$\xrightarrow{Q_{U_{\text{in}}}} \frac{-1}{2}|1\rangle \otimes |0^\perp\rangle \otimes |\varphi\rangle - \frac{\sqrt{3}}{2}|0\rangle \otimes (\quad (S40)$$

$$|01\rangle \otimes XUXU^{-1}|\varphi\rangle + \quad (S41)$$

$$|10\rangle \otimes YUYU^{-1}|\varphi\rangle + \quad (S42)$$

$$|11\rangle \otimes ZUZU^{-1}|\varphi\rangle).$$

Applying G^\dagger again. It then turns to

$$|\Psi_{\text{IV}}\rangle = |0\rangle \otimes (|00\rangle \otimes U^{-1}U^{-1}|\varphi\rangle + \quad (S43)$$

$$|01\rangle \otimes XU^{-1}XU^{-1}|\varphi\rangle + \quad (S44)$$

$$|10\rangle \otimes YU^{-1}YU^{-1}|\varphi\rangle + \quad (S45)$$

$$|11\rangle \otimes ZU^{-1}ZU^{-1}|\varphi\rangle), \quad (S46)$$

$$\xrightarrow{H^{\otimes 2}} \frac{1}{4}|0\rangle \otimes [|00\rangle \otimes 2\text{Tr}(U^{-1}) + \quad (S47)$$

$$|01\rangle \otimes (YU^{-1}Y - U) + \quad (S48)$$

$$|10\rangle \otimes (XU^{-1}X - U) + \quad (S49)$$

$$|11\rangle \otimes (ZU^{-1}Z - U)]U^{-1}|\varphi\rangle, \quad (S50)$$

$$\xrightarrow{\text{CX\&CY}} \frac{1}{4}|0\rangle \otimes [|00\rangle \otimes 2\text{Tr}(U^{-1}) + \quad (S51)$$

$$|01\rangle \otimes (U^{-1}Y - YU) + \quad (S52)$$

$$|10\rangle \otimes (U^{-1}X - XU) + \quad (S53)$$

$$|11\rangle \otimes (U^{-1}Z - ZU)]U^{-1}|\varphi\rangle. \quad (S54)$$

Since the decomposition of U on Pauli basis is $U = \cos \frac{\theta}{2}I - i \sin \frac{\theta}{2}\vec{n} \cdot \vec{\sigma}$, it can be verified

$$U^{-1}\sigma_i - \sigma_i U = 2 \sin \frac{\theta}{2}n_i I \quad (S55)$$

Finally, the output state of the circuit is

$$|\Psi_{\text{OUT}}\rangle = \frac{1}{2}|0\rangle \otimes \left(\cos \frac{\theta}{2}|00\rangle - i \sin \frac{\theta}{2}n_y|01\rangle - i \sin \frac{\theta}{2}n_x|10\rangle - i \sin \frac{\theta}{2}n_z|11\rangle \right) \otimes U^{-1}|\varphi\rangle \quad (S56)$$

■

Corollary 2 C_V in Figure S2b satisfies $C_V(U)|000, \psi\rangle = |000\rangle \otimes U^{-1}|\psi\rangle$.

Proof As shown in Figure S2b, the performance of the circuit C_V on $|000, \psi\rangle$ can be directly calculated using the same method as above, where the matrices $Q_{U_{\text{in}}}$ and G are identical to those in Figure S2a. Therefore, we omit the specific calculation details here. ■